Proc. of the International Conference on Electrical, Computer, Communications and Mechatronics Engineering (ICECCME)
7-8 October 2021, Mauritius

2021 International Conference on Electrical, Computer, Communications and Mechatronics Engineering (ICECCME) | 978-1-6654-1262-9/21/$31.00 ©2021 IEEE | DOI: 10.1109/ICECCME52200.2021.9590939

Sensing and sensing-of-sensing with drones

Steve Mann
MannLab Canada
Toronto, Canada
hydraulophone@gmail.com

Samir Khaki
MannLab Canada
Toronto, Canada
samir.khaki@mail.utoronto.ca

Jaden Bhimani
MannLab Canada
Toronto, Canada
jadenbh12@gmail.com

Gael Verges
MannLab Canada
Toronto, Canada
gael.verges@mail.utoronto.ca

Faraz Sadrzadeh-Afsharazar
MannLab Canada
Toronto, Canada
fsadrzad@ryerson.ca

***Abstract*—Vehicles such as cars, mobility scooters, wheelchairs, and the like are becoming partially or fully automated (i.e. equipped with driver-assist technologies or completely self-driving technologies). These technologies rely heavily on sensors such as vision (cameras), radar, sonar, etc..**

In this paper, we propose the use of autonomous craft (e.g. "drones") for scientific meta-measurement, i.e. specifically sensing-of-sensors and sensing their capacity to sense (metasensing). In particular, we show how a drone can be used to characterize a sonar sensing device. Sonar sensing devices are often used on autonomous vehicles.

Our two main contributions are: (1) the use of drones for the sensing of acoustic sensors (e.g. sonar transducers), and (2) minimizing the metasensing flight paths by following phase contours (i.e. vector scanning rather than raster scanning), so that a small number of flights can provide meaningful insight into the characteristics of an acoustic sensor.

***Index Terms*—Unmanned Aerial Vehicles, Acoustic Waves, Remote Sensing, Extended Reality, Phase Locked Loops**

I. BACKGROUND AND PRIOR RELATED WORK

This paper builds upon research reported in [1] which introduced the idea of using drones for sensing and metasensing (the sensing of sensors and the sensing of their capacity to sense), which had a primary focus on optical sensing and optical metasensing (e.g. the sensing of optical sensors), such as photographing, characterizing, or measuring a camera's capacity to sense.

The terms *meta*sensing, *meta*vision, *meta*veillance, etc., come from the Greek word "meta" which means "beyond" in a self-referential context, e.g. "metadata" is data about data, a meta-conversation is a conversation about conversations, etc.. Metasensing is therefore the sensing of sensing [1].

Previously reported work on metasensing has been focused on optical metasensing also known as metavision [1], i.e. visualization of vision sensors (e.g. metaveillography [1] and metaveillogrammetry [1]). Examples of metavision are shown (as prior art background) in Fig 1 and 2.

Other previous work on metasensing includes sensing of acoustic sensors [2] using hand-operated devices as well as robotic mechanisms.

In this paper we concern ourselves with acoustics and phase coherence across spatial regions. e.g., sound patterns of vibrations that create a periodic pattern of sound pressure waves propagating outwards through media from an arbitrary (e.g. localized or distributed) source or sources.

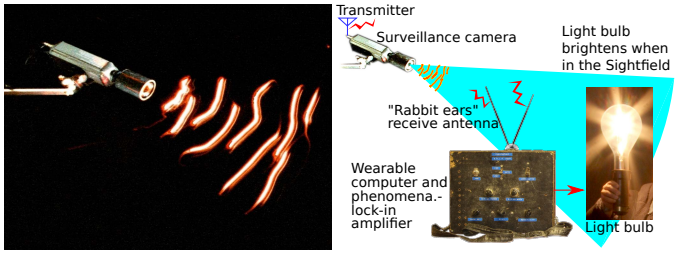

Fig. 1. Metaveillance/metavision apparatus from the mid 1970s [3]–[5] using incandescent light bulbs connected to a lock-in amplifier or television receiver. This systems allows a human observer to see the extent of coverage of a surveillance camera. The light bulb glows dim red outside the camera's field of view, but due to video feedback glows brilliantly whenever the camera can "see" it (i.e. whenever the light source is within the camera's field of view). When the light is waved back and forth in front of a surveillance camera it displays the camera's capacity to sense. This was an early form of augmented reality requiring no special eyewear. In a dark room, with the naked eye, one can see the camera's capacity to see. Figure reproduced from [1].

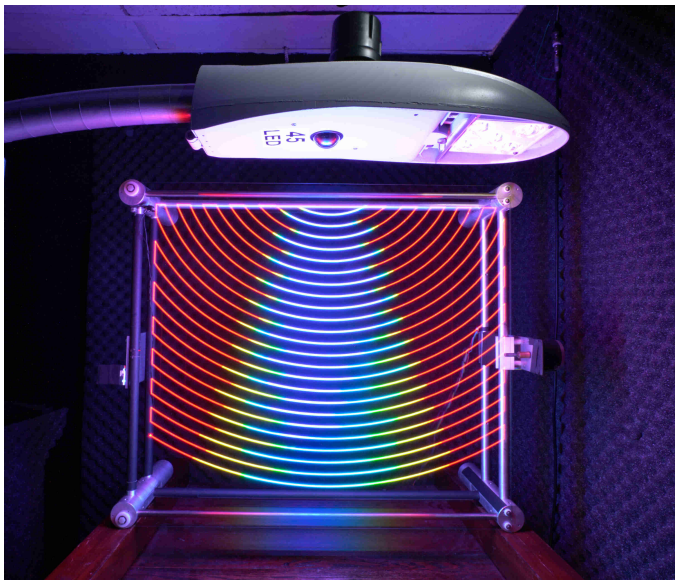

Fig. 2. Using metaveillance to show how a smart streetlight's built in camera can "see". Here the metaveillance is mechanized by way of robotics, not requiring human intervention. Instead of a human waving the light source back and forth, as was done for Fig. 1, the movement is done by a robot. Figure reproduced from [1].

This paper provides two contributions not reported elsewhere in the literature:

1) use of drones for acoustic metasensing; and
2) dynamic following of an acoustic wavefront, e.g. metasensing along a path of constant phase, minimizing the flight path by following phase contours (i.e. vector scanning rather than raster scanning), so that a small number of flights can provide meaningful insight into the characteristics of an acoustic sensor. This is in contrast to raster-scanning where the metasensing is done in a fixed pattern, usually a fixed raster in Cartesian coordinates, or a fixed raster in polar-coordinates such as in Fig. 2.

II. OVERVIEW OF SENSING-OF-SENSORS

Drone systems are proposed for metasensing purposes, i.e sensing the capacity of acoustic sensors to sense. Acoustic transducers that are typically used for sonar can transmit or receive (i.e. can function as analogous to either a "speaker" or "microphone"). We scan this transducer-under-test by using another transducer. One of the transducers is the transmit transducer and the other is the receive transducer. It has been shown that the choice of which is the transmit transducer and which is the receive transducer is arbitrary (i.e. veillogrammetry and metaveillogrammetry are reciprocals of one-another) [6]. We decided to have the transducer on the vehicle-under-test be the transmitter ("speaker") and the moving transducer be the receive transducer ("microphone") because the microphone has less mass and occupies less space, thus presenting a more modest payload.

We measure the response of a sound wave emitted from the transducer-under-test (speaker), phase-coherently, i.e. using a lock-in amplifier, as outlined in [1].

By moving the drone over a large 3D space, one can visualize the transformation of the wave over time using one or more RGB (Red, Green, Blue) LEDs to represent changes in the real and imaginary quantities output from the lock-in amplifier at different points in space. This configuration is called the Sequential Wave Imprinting Machine (SWIM), as it sequentially traces out or makes visible arbitrary periodic waveforms, typically using a light source attached to the moving transducer to visualize, in real-time, the sound wave as if it were sitting still (i.e. in spatiotemporal coordinates in which the speed-of-sound is effectively zero) [6].

In our case we use a drone to move the microphone together with an RGB LED, as shown in Fig. 3. The transmit transducer ("speaker") on the vehicle-under-test is driven by a signal generator. We tested it at various frequencies, and even a very faint signal can be picked up with the lock-in amplifier. A good lock-in amplifier can produce a gain of around 10,000,000,000 times while ignoring interference (noise such as the whir of the drone propellers) that is 1,000,000 times stronger than the signal under test. In our experiments we used a frequency of 1000Hz which has a wavelength of about 343mm at 20 deg. C, i.e. 1000Hz/(343m/s). Thus the pattern of the sound wave repeats every 343mm as the drone flies the RGB LED around in the space.

Unlike other robotic movement devices, drones offer a critical advantage as they operate autonomously and require minimal external hardware setup for positioning, and they can fly into small confined spaces that robots sometimes have difficulty reaching into. Once the drone's position has been calibrated, it can trace out sound waves with centimetre level precision. The drone can fly either a Cartesian raster, polar raster, or fly along the lines of constant phase where the $\arctan(\text{real}/\text{imaginary})$ does not change as shown in Fig. 11, i.e. fly in a vector pattern rather than a raster.

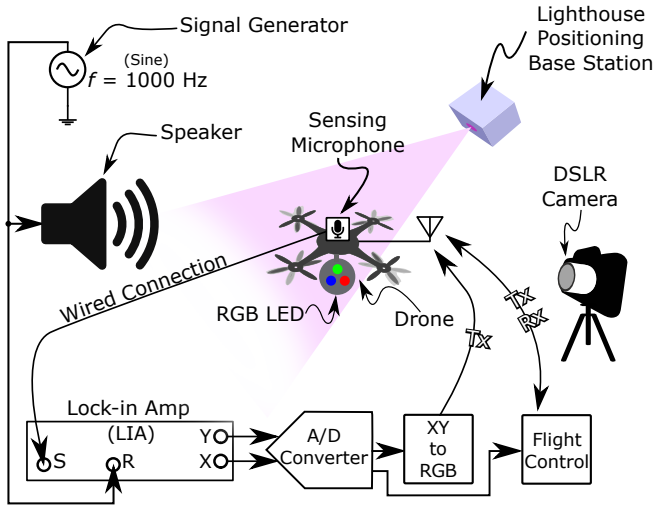

Fig. 3. System setup for testing acoustic sonar. The transmit transducer (speaker) is driven by a test signal fed to the reference input of a lock-in amplifier (LIA). A microphone on the drone is connected to the signal input of the LIA. The real-valued output XO and imaginary-valued output YO of the lock-in amplifier are captured with an A/D converter and the resulting complex-valued quantity is converted to LED colour as outlined in [4], [6], [7]. The data from the LIA together with the flight control are captured in sync, i.e. as (x,y,z,XO,YO) for each point in space, sampling at 20 microseconds (i.e. 50,000 samples per second). A long-exposure photograph is also captured during the run, so that we can compare the physical reality with the virtual (3-D rendered) data. Drone and speaker symbols were taken from WikiMediaCommons Images.

III. DRONES FOR ACOUSTIC SENSING

We accomplish the sensing of acoustic sensors through a system that enables the visualization of acoustic vibration patterns using both photographic imagery (by way of photography or by way of direct viewing of moving light sources with human vision) as well as computational rendering (e.g. computer graphics). Photographs are appealing, as evidence, to judges, juries, and courtrooms. Despite the fact that photographs can be altered, they nevertheless are often considered as evidence in contrast to the descriptive testimony of expert data [1]. The photographic results are obtained using a combined hardware-software approach to the Sequential Wave Imprinting Machine (SWIM) [6] to visualize the metasensing [6], [8], [9]. Thus for example we can provide photographic evidence that a sensor in a vehicle was in good working order when it left the factory or a service centre. We have used this approach to test motor vehicles, e.g. when testing the Ford Focus electric vehicle sensor systems, we can use a photographic darkroom booth open at both ends so that cars can drive in, be tested, and then

drive out (like an assembly-line) [1], as depicted in Fig. 4. In addition to producing the photographs, we also capture a richly intricate dataset showing the function and efficacy of the acoustic sensor. This dataset (as well as the photographs, i.e. using computational photography, as outlined in United States patent numbers 10,540,014, 10,168,791, and 9,720,505) is visualized in 3-dimensions using virtual reality, or using augmented reality to see it overlaid on top of the car itself.

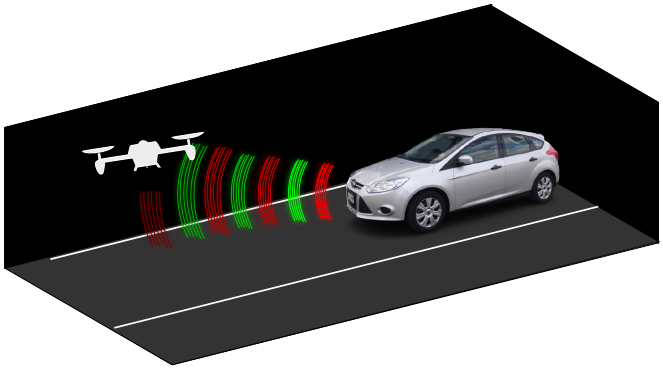

Fig. 4. Computer-generated depiction of the flight path and color shifting of the metasensing (metaveillance flux [10]) on a Ford Focus. The drone SWIMs along regions of constant phase at periodic intervals thus showing a decrease in luminosity as the drone moves further from the acoustic source. The continuity of color along each region of constant phase demonstrates the capacity of sensing. Drone Icon and Ford Car taken from WikiMediaCommons Images.

The metasensing of vehicular sensors can be applied to a wide variety of acoustic, optical and spatial sensors. In this paper we concentrate specifically on acoustic sensors. The drone-based apparatus (that is part of the overall acoustic metasensing system) is comprised of the following elements: the Crazyflie™2.1 Drone System, the Crazyflie™LED Deck, and our own custom-designed (computational) PID Controller. PID (Proportional, Integral, Derivative) controllers are well-known in the art, i.e. as a control system that responds to position ("P"), absement ("I" which is the integral of position), and velocity ("D" which is the derivative of position). See Fig. 4 illustrating a three dimensional rendering of the proposed drone-based apparatus applied towards vehicular testing.

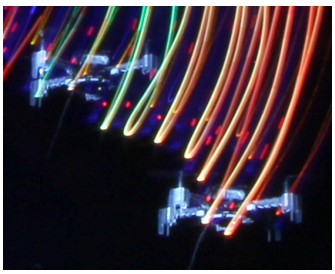

Fig. 5. Close-up long-exposure photograph of drone transforming Acoustic Information into the visual spectrum using SWIM facilitated via the LED Deck on the drone.

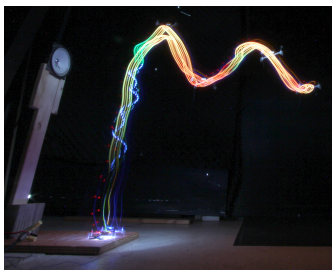

Fig. 6. Long-exposure photograph detailing the drone's SWIM relative to the equipment setup of the speaker. The drone is flying in a wave pattern outward from the acoustic source to SWIM out spatial phase distribution using its fastened LED Deck.

A. Drone System

The Drone System is presented as a cohesive unit integrated with the Crazyflie 2.1 responsible for tracking acoustic interactions over space, illustrated in Fig. 5 and 6.

1) Flight Controller: The flight controller for the Crazyflie 2.1 contains an on-board radio and the PDB (power distribution board), both controlled by an RF51822 micro controller [11]. The on-board radio operates at 2.4GHz (ISM band) connecting the Crazyradio PA (Public address) USB dongle enabling lossless, low-latency communication with the drone [12] for sending command packets including LED colour changes and positional adjustments [13]. The integrated PDB allows the drone to operate independent of ESCs (electronic speed controllers) or signal wires to the motors [14]. During operation, the drone processes inputs from the lighthouse deck, internal gyroscope, and client connection with the STM32F405 168MHz main application micro controller [11].

To be able to accurately depict invisible phenomena, the flight path of the drone is determined algorithmically and sent as a series of commands via the radio dongle connected to the ground control station (laptop). In order to dynamically set its flight path, the Crazyflie python library (cflib) was installed in the development environment, enabling the initialization and sending of specific setpoints for the drone to fly to [13]. By running an iterative loop and sending hundreds of commands every second, the drone was able to seamlessly and smoothly fly across a locus of points, such as a simple raster with colour shifts to visualize the 1000Hz signal being emitted, or fly along a path of constant phase (vector rather than raster graphics).

2) Multimeters and Amplifier Setup: On-board the drone system is a microphone connected with a twisted pair to the lock-in amplifier, for measuring acoustic response. The lock-in-amplifier produces both real and imaginary outputs which are fed via coaxial cables fitted with BNC connectors into two Keysight 34470a digit multimeters to perform A/D conversion. The Keysight multimeters were selected on the basis of easy integration with regards to compatibility for remote triggering using the standard Virtual Instrument Software Architecture (VISA) API [15], [16]. With the multimeters connected over a serial port through USB 2.0 cables, a PyVISA (python implementation of VISA) [17] script was developed to remotely trigger both multimeters every 20 microseconds [18] and record the latest data point. The recorded data was stored as floating points to preserve measurement precision. It was written into two .txt files - one for each input component (real and imaginary). These text files were parsed via a python script extracting phase values for the LED Deck and PID controller thus connecting all drone systems for an adaptive positioning and color shifting routine.

3) Positioning System: The positioning system follows from the mapping of the environment to ensure drone alignment and orientation for maintaining positional accuracy over the space. The positioning system was powered by a lighthouse comprised of a base station and drone-mounted lighthouse deck. A single HTC Vive v1.0 base station was suspended 4 metres off the ground pointing downwards at an angle of 45

degrees. While two are recommended, one base station was used for the current experiment so as to not have the vehicle of origin blocking any light from the lighthouse deck [19]. The base station sends out an IR (InfraRed) laser beam in two dimensions across the entire room (commonly referred to as its "flash") that is detected by all sensors on the lighthouse deck at the same time, then conducts two sweeps of the room: one horizontal and one vertical [20]. The second part of the system is the lighthouse deck, which is fitted to the flight controller and acts as its primary point of reference for positioning [14].

To maintain accuracy, the system requires two sets of data: the calibration data describing any imperfections or adjustments made to the base station, and the geometry data which uses the IR sweeps to estimate the position of the lighthouse in relation to the drone [19]. Geometry data is collected at the beginning of every test using the Crazyflie python GUI client (cfclient) which combines the lighthouse estimations with the drone's internal gyroscope data to create a three dimensional rendering of the location of the drone and lighthouse in OpenGL. The rendering forms a 3D Cartesian coordinate system from which a set of specific setpoints can be selected for the drone to autonomously navigate to [13]. The drone's starting position is set at the origin of the coordinate system scaled such that 1 unit in the Cartesian space represents 1 metre in physical space. For positional control, the drone's movement was limited to an order of magnitude in the decimetre range.

B. LED Deck

The Crazyflie™ LED-ring expansion deck was mounted onto the Crazyflie 2.1 drone's pin headers and was controlled by a python script. The LED deck is comprised of 12 RGB LEDs thus enabling visualization of a full color spectrum in response to phase angle measurements recorded at the drone's location in space. Each phase measurement was normalized to an RGB value within the range of 0 to 255 so as to display the spatial phase and quantity distribution. This algorithmic approach was inspired from [6] where it was used in a variety of SWIM applications from the sampling of meta wave functions to spatially distributed phenomena [7]. The algorithm works by dividing the Argand (complex) plane into regions of phase as shown in Fig. 7. A red to green crossfade is calculated for phase angles in the $[0°$ to $180°)$ region, a green to blue crossfade in the $180°$ to $270°$ region and a blue to red crossfade in the $270°$ to $360°$ region. The values obtained for red, green, and blue from the crossfades are multiplied by the magnitude of the lock-in amplifier's output normalized in the range [0,1] multiplied by 255.99, to yield the RGB values.

The cumulative result of the applied color shifting on the drone is visualized in Fig. 10 where as the drone moves further from the source, it shows different regions of phase in a continuous motion. As the drone travelled away from the source over time, a DSLR Long Exposure Camera was able to capture the visually traced out pattern creating the phase distribution photo in Fig. 10. To examine the phase coherence of the Acoustic space, further advancements were made to augment the sensing of the drone and the visual results tracing that it offered. Particularly, the use of an adaptive PID controller allowed the drone to not only illustrate color continuity across phase, but also phase coherence over the acoustic space.

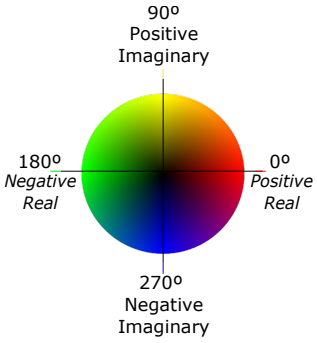

Fig. 7. Color wheel superimposed on the Argand (complex) plane. The color encoding is used to determine RGB values corresponding to the measured phase angles, inspired from [7].

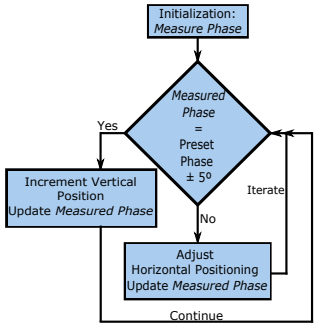

Fig. 8. Flowchart depicting PID controller for phase-coherent flight paths. The iterative nature of the controller ensures a constant phase lock-in of the target at each vertical increment.

C. PID Controller

A PID controller was implemented as a proportional-only feedback algorithm to modulate the drone flight path over the acoustic space - see Fig. 8. As an adaptive system, the controller moves the drone towards a preset phase along the locus of points defined by that constant phase. The drone measures the current phase value at its position and adjusts its flight path by an amount proportional to the error bound between the current phase angle and the target phase. The flight path is adjusted along the horizontal plane in order to guarantee that at any given height along the drone's flight path, it will be tracking the predefined phase path. A key feature of the proportional based PID controller is the iterative nature of flight path adjustment. At each increment in the vertical direction, the drone will iterate through several proportional adjustments of horizontal position until the measured phase has achieved the target phase within a 5 degree tolerance range. By iterating the adjustments at each height, the control system is able to guarantee that the drone's location accurately depicts the regions of constant phase in the acoustic space. The efficacy of the PID control system is well illustrated in Fig. 11.

IV. Drone Vision

The proposed method of using drones to trace out acoustic meta-sensing through both color shifting and flight path control presents a novel approach to asses sonar rigs. A general procedure was adapted and subsequently employed to create Figs. 9, 10, and 11 such that they can describe the underlying relationships of the sonar rig from an autonomous vehicle - as it interacts in the acoustic space. A general procedure outlined below details the commonality in flight methodology across the three different drone tests. The differences in both flight path and camera procedure are also outlined below in their respective sections.

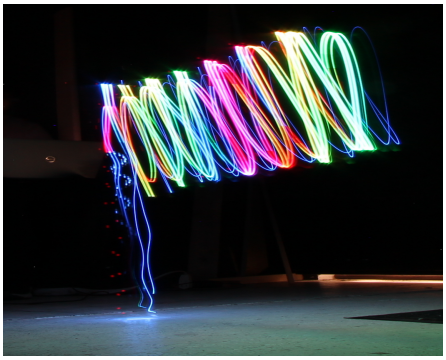

Fig. 9. Long-exposure photo of drone flying high-frequency sine wave pattern while moving away from speaker. Phase angle of detected sound wave is indicated by colour of LED.

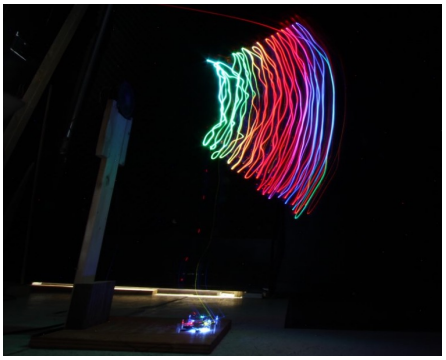

Fig. 10. Long-exposure photo taken of drone flying in 70° arcs while moving away from a speaker. Phase indicated as per colour wheel of Fig. 7).

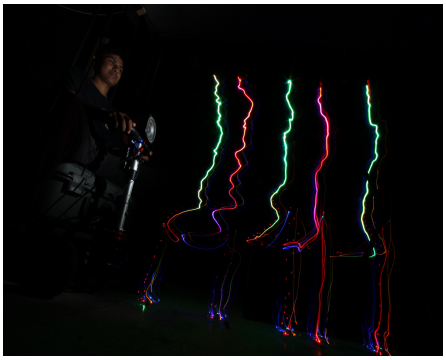

Fig. 11. Multi-exposure photo of drone using PID controller to fly path of constant phase. Horizontal flight path constantly adjusted to find desired phase. Green represents 180° phase, red 0°.

A. General Procedure

The drone is placed on the ground, on a line orthogonal to the speaker, oriented such that its starboard side is nearest the speaker. The operator, seated behind the acoustic source, performs the lighthouse-drone calibration procedure using the cfclient software. This procedure includes drone calibration and re-acquiring the geometry data between the drone and the lighthouse so as to set the origin of the Cartesian plane. Following geometry acquisition, a python script collects data from the multimeters via a GPIB interface, at which point one of the three flight tests is executed. During the test, both the multimeter and drone piloting scripts run concurrently so as to constantly update the LED colour with its associated phase angle at every point in space while simultaneously providing input to the PID controller for positional adjustment. To capture results, a DSLR camera is calibrated for long exposure in the dark environment. Once the camera positioning is set, it remains in place for the duration of each individual set of tests so as to ensure sequence coherence across multiple exposures of images. Light flashes (xenon flash lamp) are performed to illuminate the environment on each individual photo such that it can be seen in the final long exposure. Upon completion of the piloting script the drone returns to its original starting position through a predefined landing protocol. A maximum ceiling height constraint was applied to all tests with a value of 1.0 m to ensure that the drone stays within a 120 degree range of the lighthouse.

B. Cartesian-Raster-Specific Adaptation

The piloting script for the raster specific test used operates the drone along a predefined flight path in the form of a high-frequency high-amplitude sine wave as shown in Fig. 9

C. Polar-Raster-Specific Adaptation

This piloting script - results in Fig. 10 - operates the drone along a predefined positional flight path of the form:

$$\begin{cases} x = A \cdot t \\ y = B \cdot \sin(2\pi \cdot f \cdot t) + C \end{cases} \qquad f = 80\,\text{cycles/metre}$$

In this case, the horizontal positioning increases incrementally over time while the vertical position traces out a repetitive sin function path. The drone begins at a minimum height of 0.4 m. Over the course of this test, the drone flies a series of 55 cycles alternating upward and downward with an effective angular arc of 70º relative to the center of the acoustic source placed at a height of 0.58 m. Upon test completion, the drone returns to standard landing protocols outlined in the General Procedure. The overall test is recorded as a single long exposure photograph with the DSLR shutter remaining open as the drone progresses through its flight path.

D. Vector-Specific Adaptation

For the case of the vector phase-front piloting script, the drone initially flies up to a height of 0.3 m and proceeds to follow the constant-phase curve with horizontal adjustments occurring at each vertical increment up until a ceiling height of 0.98 m. The positional adjustments at each vertical increment are defined by the PID Controller in Fig. 8 and as such, there was no external pre-programming for this test, making it the most adaptive and responsive to self-modulated sensing in comparison with the previous tests. Each phase-front is drawn as an individual test after which the drone follows its landing protocols. As such, the phase front curves had to be combined to output the results in Fig. 11. Unlike the previous tests, the phase-front graph must contain a sequence of arcs across different flights. To accomplish this, an initial base vector imaging is completed by flashing a high powered light at the base while capturing photos, after which each subsequent run is simply captured as an individual long exposure photo. After all runs are complete, a photo stacking algorithm is employed to combine the images into a single photograph. Since the camera is stationary and the surrounding environment is unchanging, the images stack perfectly, creating a long exposure image over both space and time - see Fig. 11.

V. RESULTS AND DISCUSSION

Drones have proven to be very well suited to acoustic sensing thanks to their ability to navigate through 3D space in a precise and stable manner when used in conjunction

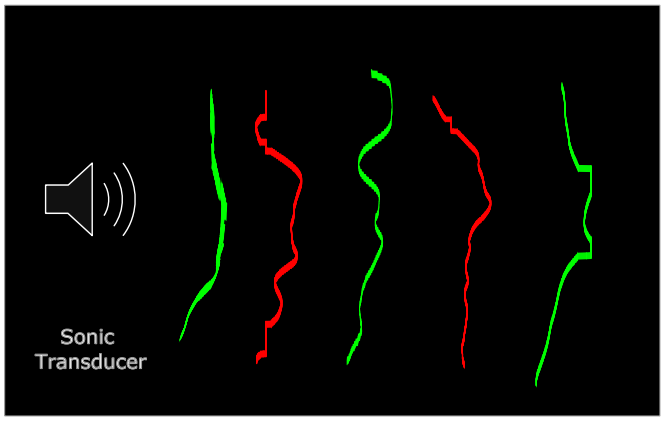

Fig. 12. Computer-generated depiction of the flight path traced from the positional coordinates of the drone provided by the PID controller. Speaker Icon taken from WikiMediaCommons Images.

with an external "lighthouse" positioning system while being controlled by a script running on a computer. It has been shown above that the drone is able to either SWIM out predetermined patterns to provide a visual depiction of the phase spatial distribution, but also to follow curves of constant phase using a PID controller. This latter task is of particular importance as it is a distinctive quality of autonomously-controlled devices such as drones. It would be very difficult to accurately and reliably SWIM out a locus of points of constant phase using a handheld SWIM. Furthermore, the drone's great adaptability makes it even more suited to SWIM purposes. In this case, the drone carried an LED deck for phase representation but also a microphone connected via wire to the lock-in amplifier. It is perfectly possible for the drone to carry other sensors than a microphone as well, thus increasing its applicability to a wide variety of metasensing-related tasks.

To illustrate the drone's spatial accuracy, Fig. 12 shows the path which the drone actually traced out based on computed coordinate values while Fig. 11 is a photograph showing the trace as apparent in reality. There was some oscillation attributed to the lighthouse but the overall trends of each curve are fairly consistent further bolstering the efficacy of the autonomous drones.

There is without doubt a myriad of future applications for drones in metasensing applications thanks to their ability to both follow preset paths in a very precise manner, and their capacity to follow a locus of points corresponding to a particular feature of a spatial distribution.

VI. Conclusion

This paper introduced a novel approach to metasensing of acoustic space through the use of autonomous craft. The proposed method creates a visualization of an otherwise invisible phenomenon by tracing out relations of the acoustic space into an AR. The three tests employed in this paper included the Cartesian raster, polar raster, and phase-front arcs. From an evolutionary perspective, these three tests build up an autonomous craft capable of self directing its path along regions of constant phase while illustrating its precision through the accuracy of the color shifting. With applications in autonomous vehicles, the drones present an efficient and versatile approach to the characterization of sonar based systems and their interactions within the environment.

ACKNOWLEDGMENT

The authors thank the many advisors, affiliates, and students of MannLab and MannLab Canada as well as members of SwimOP = Swim at Ontario Place (informally "Ontario Place University" and "Teach Beach™") where we are developing underwater versions of this technology to sense water quality through machine learning of acoustic transmission properties.

REFERENCES

[1] S. Mann, C. Pierce, J. Hernandez, Q. Li, B. Cong, and Y. X. Xiang, "Drone swarms for Sensing-of-Sensing," *IEEE Sensors*, pp. 1–4, Aug. 2019.
[2] S. Mann, "Surveillance, sousveillance, and metaveillance," pp. 1408–1417, CVPR2016.
[3] ——, "Phenomenal augmented reality: Advancing technology for the future of humanity," *IEEE Consumer Electronics*, pp. cover + 92–97, October 2015.
[4] ——, "Wavelets and chirplets: Time–frequency perspectives, with applications," in *Advances in Machine Vision, Strategies and Applications*, world scientific series in computer science - vol. 32 ed., P. Archibald, Ed. Singapore . New Jersey . London . Hong Kong: World Scientific, 1992.
[5] "Steve Mann," *Campus Canada, ISSN 0823-4531, p55 Feb-Mar 1985, pp58-59 Apr-May 1986, p72 Sep-Oct 1986*.
[6] S. Mann, "Phenomenological augmented reality with swim," pp. 220–227, 2018.
[7] ——, ""Rattletale": Phase-coherent telekinetic imaging to detect tattletale signs of structural defects or potential failure," *SITIS 2017, SIVT4: Theory and Methods*.
[8] P. Scourboutakos, M. H. Lu, S. Nerker, and S. Mann, "Phenomenologically augmented reality with new wearable led sequential wave imprinting machines," in *Proc. ACM TEI*. ACM, 2017, pp. 751–755.
[9] S. Mann, T. Furness, Y. Yuan, J. Iorio, and Z. Wang, "All reality: Virtual, augmented, mixed (x), mediated (x, y), and multimediated reality," *arXiv preprint arXiv:1804.08386*, 2018.
[10] R. Janzen and S. Mann, "Vixels, veillons, veillance flux," *IEEE CCECE*, pp. 1–10, 2014.
[11] "Datasheet crazyflie 2.1 - rev 1." [Online]. Available: https://www.bitcraze.io/documentation/hardware/crazyflie_2_1/crazyflie_2_1-datasheet.pdf
[12] crazyflie, "Development overview." [Online]. Available: https://www.bitcraze.io/development/development-overview/
[13] "The crazyflie python api." [Online]. Available: https://www.bitcraze.io/documentation/repository/crazyflie-lib-python/master/user-guides/python_api/
[14] "Crazyflie platform overview." [Online]. Available: https://www.bitcraze.io/documentation/system/platform/
[15] "Digital multimeters 34460a, 34461a, 34465a (6½ digit), 34470a (7½ digit)." [Online]. Available: https://www.keysight.com/ca/en/assets/7018-03846/data-sheets/5991-1983.pdf
[16] Keysight, "I/O libraries example programs," Jan 2021. [Online]. Available: https://www.keysight.com/ca/en/lib/software-detail/programming-examples/io-libraries-example-programs-2798637.html
[17] "Control your instruments with python¶." [Online]. Available: https://pyvisa.readthedocs.io/en/stable/
[18] Keysight, "Bench truevolt dmms," Sep 2020. [Online]. Available: https://www.keysight.com/ca/en/products/digital-multimeters-dmm/truevolt-series-multimeters.html
[19] "Lighthouse system overview." [Online]. Available: https://www.bitcraze.io/documentation/repository/crazyflie-firmware/2021.03/functional-areas/lighthouse/system_overview/
[20] "Lighthouse positioning system: Dataset, accuracy, and precision for UAV research." [Online]. Available: https://arxiv.org/pdf/2104.11523.pdf